Imaging carious dental tissues with multiphoton fluorescence lifetime imaging microscopy

Po-Yen Lin,[1,2] Hong-Chou Lyu,[1] Chin-Ying Stephen Hsu,[3,6] Chia-Seng Chang,[2] and Fu-Jen Kao[1,4,5]

[1]*Institute of Biophotonics, National Yang-Ming University, Taipei 11221, Taiwan*
[2]*Institute of Physics, Academia Sinica, Taipei 11529, Taiwan*
[3]*Department of Preventive Dentistry, Faculty of Dentistry, National University Health System, National University of Singapore, Singapore 119074*
[4]*Department of Photonics, National Sun Yat-sen University, Kaohsiung 80424, Taiwan*
[5]*fjkao@ym.edu.tw*
[6]*chin-ying_stephen_hsu@nuhs.edu.sg*

Abstract: In this study, multiphoton excitation was utilized to image normal and carious dental tissues noninvasively. Unique structures in dental tissues were identified using the available multimodality (second harmonic, autofluorescence, and fluorescence lifetime analysis) without labeling. The collagen in dentin exhibits a strong second harmonic response. Both dentin and enamel emit strong autofluorescence that reveals in detail morphological features (such as dentinal tubules and enamel rods) and, despite their very similar spectral profiles, can be differentiated by lifetime analysis. Specifically, the carious dental tissue exhibits a greatly reduced autofluorescence lifetime, which result is consistent with the degree of demineralization, determined by micro-computed tomography. Our findings suggest that two-photon excited fluorescence lifetime imaging may be a promising tool for diagnosing and monitoring dental caries.

OCIS codes: (170.1850) Dentistry; (170.3880) Medical and biological imaging; (170.6935) Tissue characterization; (170.6920) Time-resolved imaging.

References and links

1. A. R. Ten Cate, *Oral Histology 3rd ed.* (Mosby, St. Louis, 1998), Chap. 5.
2. F. J. Kao, "The use of optical parametric oscillator for harmonic generation and two-photon UV fluorescence microscopy," Microsc. Res. Tech. **63**(3), 175–181 (2004).
3. S. Y. Chen, C. Y. Hsu, and C. K. Sun, "Epi-third and second harmonic generation microscopic imaging of abnormal enamel," Opt. Express **16**(15), 11670–11679 (2008).
4. L. Bachmann, D. M. Zezell, A. da Costa Ribeiro, L. Gomes, and A. S. Ito, "Fluorescence spectroscopy of biological tissue-A review," Appl. Spectrosc. Rev. **41**(6), 575–590 (2006).
5. A. Zoumi, A. Yeh, and B. J. Tromberg, "Imaging cells and extracellular matrix in vivo by using second-harmonic generation and two-photon excited fluorescence," Proc. Natl. Acad. Sci. U.S.A. **99**(17), 11014–11019 (2002).
6. W. R. Zipfel, R. M. Williams, R. Christie, A. Y. Nikitin, B. T. Hyman, and W. W. Webb, "Live tissue intrinsic emission microscopy using multiphoton-excited native fluorescence and second harmonic generation," Proc. Natl. Acad. Sci. U.S.A. **100**(12), 7075–7080 (2003).
7. P. J. Campagnola, and L. M. Loew, "Second-harmonic imaging microscopy for visualizing biomolecular arrays in cells, tissues and organisms," Nat. Biotechnol. **21**(11), 1356–1360 (2003).
8. P. J. Campagnola, A. C. Millard, M. Terasaki, P. E. Hoppe, C. J. Malone, and W. A. Mohler, "Three-dimensional high-resolution second-harmonic generation imaging of endogenous structural proteins in biological tissues," Biophys. J. **82**(1), 493–508 (2002).
9. M. H. Chen, W. L. Chen, Y. Sun, P. T. Fwu, and C. Y. Dong, "Multiphoton autofluorescence and second-harmonic generation imaging of the tooth," J. Biomed. Opt. **12**(6), 064018 (2007).

#137507 - $15.00 USD Received 2 Nov 2010; revised 7 Dec 2010; accepted 16 Dec 2010; published 17 Dec 2010

10. K. Koenig, and H. Schneckenburger, “Laser-induced autofluorescence for medical diagnosis,” J. Fluoresc. **4**(1), 17–40 (1994).
11. V. V. Ghukasyan, and F. J. Kao, “Monitoring cellular metabolism with fluorescence lifetime of reduced nicotinamide adnine dinucleotide,” J. Phys. Chem. **113**, 11532–11549 (2009).
12. K. Koenig, R. Hibst, G. Flemming, and H. Schneckenburger, “Laser-induced autofluorescence of caries,” Proc. SPIE **1880**, 125–131 (1993).
13. R. Hibst, R. Paulus, and A. Lussi, “Detection of occlusal caries by laser fluorescence: basic and clinical investigations,” Med. Laser Appl. **16**(3), 205–213 (2001).
14. E. Borisova, T. Uzunov, and L. Avramov, “Laser-induced autofluorescence study of caries model in vitro,” Lasers Med. Sci. **21**(1), 34–41 (2006).
15. R. R. Gallagher, S. G. Demos, M. Balooch, G. W. Marshall, Jr., and S. J. Marshall, “Optical spectroscopy and imaging of the dentin-enamel junction in human third molars,” J. Biomed. Mater. Res. A **64A**(2), 372–377 (2003).
16. W. Becker, A. Bergmann, M. A. Hink, K. König, K. Benndorf, and C. Biskup, “Fluorescence lifetime imaging by time-correlated single-photon counting,” Microsc. Res. Tech. **63**(1), 58–66 (2004).
17. J. R. Lakowicz, Principles of fluorescence spectroscopy, 3rd edition. (New.York: Plenum Press, 2006)
18. V. V. Ghukasyan, Y. Y. Hsu, S. H. Kung, and F. J. Kao, “Application of fluorescence resonance energy transfer resolved by fluorescence lifetime imaging microscopy for the detection of enterovirus 71 infection in cells,” J. Biomed. Opt. **12**(2), 024016 (2007).
19. C. Hille, M. Lahn, H.-G. Löhmannsröben, and C. Dosche, “Two-photon fluorescence lifetime imaging of intracellular chloride in cockroach salivary glands,” Photochem. Photobiol. Sci. **8**(3), 319–327 (2009).
20. K. M. Hanson, M. J. Behne, N. P. Barry, T. M. Mauro, E. Gratton, and R. M. Clegg, “Two-photon fluorescence lifetime imaging of the skin stratum corneum pH gradient,” Biophys. J. **83**(3), 1682–1690 (2002).
21. H. C. Gerritsen, R. Sanders, A. Draaijer, C. Ince, and Y. K. Levine, “Fluorescence lifetime imaging of oxygen in living cells,” J. Fluoresc. **7**(1), 11–15 (1997).
22. S. E. D. Webb, S. Leveque-Fort, D. S. Elson, J. Siegel, T. Watson, M. J. Lever, M. Booth, R. Juskaitis, M. A. A. Neil, L. O. Sucharov, T. Wilson, and P. M. W. French, “Wavelength-resolved 3-dimensional fluorescence lifetime imaging,” J. Fluoresc. **12**(2), 279–283 (2002).
23. G. McConnell, J. M. Girkin, S. M. Ameer-Beg, P. R. Barber, B. Vojnovic, T. Ng, A. Banerjee, T. F. Watson, and R. J. Cook, “Time-correlated single-photon counting fluorescence lifetime confocal imaging of decayed and sound dental structures with a white-light supercontinuum source,” J. Microsc. **225**(2), 126–136 (2007).
24. F. Ferretti de Oliveira, A. S. Ito, and L. Bachmann, “Time-resolved fluorescence spectroscopy of white-spot caries in human enamel,” Appl. Opt. **49**(12), 2244–2249 (2010).
25. C. L. Darling, and D. Fried, “Real-time near IR (1310 nm) imaging of CO2 laser ablation of enamel,” Opt. Express **16**(4), 2685–2693 (2008).
26. G. K. Stookey, “Quantitative light fluorescence: a technology for early monitoring of the caries process,” Dent. Clin. North Am. **49**(4), 753–770, vi (2005).
27. P. T. C. So, C. Y. Dong, B. R. Masters, and K. M. Berland, “Two-photon excitation fluorescence microscopy,” Annu. Rev. Biomed. Eng. **2**(1), 399–429 (2000).
28. F. Helmchen, and W. Denk, “Deep tissue two-photon microscopy,” Nat. Methods **2**(12), 932–940 (2005).
29. U. Hafström-Björkman, F. Sundström, and J. J. ten Bosch, “Fluorescence in dissolved fractions of human enamel,” Acta Odontol. Scand. **49**(3), 133–138 (1991).
30. W. Buchalla, “Comparative fluorescence spectroscopy shows differences in noncavitated enamel lesions,” Caries Res. **39**(2), 150–156 (2005).
31. K. König, H. Schneckenburger, and R. Hibst, “Time-gated in vivo autofluorescence imaging of dental caries,” Cell. Mol. Biol. (Noisy-le-grand) **45**(2), 233–239 (1999).
32. A. Banerjee, and A. Boyde, “Autofluorescence and mineral content of carious dentine: scanning optical and backscattered electron microscopic studies,” Caries Res. **32**(3), 219–226 (1998).
33. W. Buchalla, “Comparative fluorescence spectroscopy shows differences in noncavitated enamel lesions,” Caries Res. **39**(2), 150–156 (2005).
34. C. Robinson, R. C. Shore, S. J. Brookes, S. Strafford, S. R. Wood, and J. Kirkham, “The chemistry of enamel caries,” Crit. Rev. Oral Biol. Med. **11**(4), 481–495 (2000).
35. M. V. Swain, and J. Xue, “State of the art of Micro-CT applications in dental research,” Int. J. Oral Sci. **1**(4), 177–188 (2009).
36. T. T. Huang, A. S. Jones, L. H. He, M. A. Darendeliler, and M. V. Swain, “Characterisation of enamel white spot lesions using X-ray micro-tomography,” J. Dent. **35**(9), 737–743 (2007).

#137507 - $15.00 USD Received 2 Nov 2010; revised 7 Dec 2010; accepted 16 Dec 2010; published 17 Dec 2010

37. N. Efeoglu, D. Wood, and C. Efeoglu, "Microcomputerised tomography evaluation of 10% carbamide peroxide applied to enamel," J. Dent. **33**(7), 561–567 (2005).

1. Introduction

Dental caries is one of the most common diseases throughout the world with immense social-economical impact. Bacteria are mainly responsible for initiating caries through producing acid as the metabolic products after consuming carbohydrates. Dental caries is characterized by demineralization and the degeneration of organic matrix that could cause the damage of the dental tissue. The human tooth is highly mineralized tissue, in which enamel forms the outer layer of a tooth and is the most mineralized tissue in the body. The primary mineral in enamel is hydroxyapatite, which is a crystalline calcium phosphate and forms enamel rods or prisms of size approximately 4-6 μm in transverse dimension [1]. The boundary between rods and interred enamel is delimited by rod sheath (an organic material), which causes the index mismatch and generates good contrast under third harmonic generation (THG) [2,3]. Dentin is the relatively elastic structure between enamel and the central pulp chamber. The main organic matrix in dentin is the fibrous collagen [4], which generates intense second harmonic and autofluorescence (AF) signals [5–8]. Theses optical signals could be used to visualize detailed structures of dental sections, such as dentinal tubules and enamel rods [2,3,9], and reflect the condition of dental tissue [10]. Many endogenous fluorophores are used for revealing crucial structural and functional information of tissues. For example, the reduced nicotinamide adenine dinucleotide (NADH) is a useful probe in monitoring cellular metabolism [11]. The spectra of autofluorescence from teeth in normal and pathological conditions have also been used for caries diagnosis [12–14]. However, intensity-based diagnostic tools generally suffer from fluctuation in laser intensity, concentration of confounding fluorophores, and scattering of light, which prevents precise characterization. The autofluorescence from dentin and enamel exhibit similar spectral profiles and are difficult to distinguish spectrally [15]. Nonetheless, they can be differentiated with fluorescence lifetime analysis [16]. The measurement of fluorescence lifetime has been found to be an effective way to decipher critical information on molecular dynamics, such as molecular conformation and the changes in nano-environment due to the interactions with solvent and other molecules [17,18]. It has been widely used in mapping pertinent cellular parameters, including ion concentration [19], pH of the environment [20], and oxygen saturations [21]. It has also been demonstrated that fluorescence lifetime imaging microscopy (FLIM) has the ability to distinguish the carious region from sound dental tissue [22–24]. However, using single-photon excitation at the wavelength in visible region is difficult to penetrate the dental tissue due to strong scattering [25], making it difficult to reveal carious process beneath the dental surface where the initial lesions usually start [26]. Two-photon excitation has been demonstrated as a promising technique for tissue autofluorescence imaging that has the advantages of deeper penetration and reduced photodamage [27,28].

In this study, two-photon FLIM is used to image the complex morphologic features of dental sections without denaturing samples. Different sites of a carious tooth with various level of demineralization exhibit greatly reduced autofluorescence lifetime, which is substantiated by the trend revealed in the quantification of mineral density carried out via X-ray micro-CT. Our results suggest that two-photon excited fluorescence lifetime imaging may be promising in clinical diagnosis of dental caries.

2. Materials and methods

Nine dental samples were investigated in this study, including five dental sections and four carious dental samples. Dental sections with a thickness of 150 μm were cut from a human molar using a hard tissue microtome. These sections are lightly moisturized to prevent cracking by dehydration. The carious teeth were extracted owing to clinical indication, with the approval

#137507 - $15.00 USD Received 2 Nov 2010; revised 7 Dec 2010; accepted 16 Dec 2010; published 17 Dec 2010

of the Institutional Review Board (IRB). To maintain their integrity and pristine state, no further feature-altering treatments, such as grinding, decalcifying with acid, or labeling with dyes, were applied. The sections were attached to a glass slide in a PBS buffer before observation. 2p-FLIM measurements were made using a modified Olympus FV300 confocal system with excitation by a mode-locked femtosecond Ti:Sapphire laser (Mira 900, Coherent), which was tuned to 750 nm [10]. The laser beam was coupled into the Olympus FV300 confocal scan unit and an inverted microscope (IX81, Olympus) that was equipped with the objectives (UPlanFLN 40X/NA 1.3 and UPlanSApo 10X/NA 0.4, Olympus). The average laser power at the focal plane of the objective was kept below 5 mW to prevent photodamage to the samples. The modified confocal system was capable of both forward and backward detection, as described previously [2,10]. A fiber-coupled miniature spectrometer (QE65000, Ocean Optics) was integrated into the system to facilitate spectroscopic analysis. A short pass dichroic mirror (675 DCSP, Chroma) and a band pass filter (HQ 500/140, Chroma) were used to separate the scattered laser light from autofluorescence in the backward direction. The signals were detected using a photon counting photomultiplier (PMA series, Picoquant) and, which was coupled to the TSCPC module (TimeHarp 200, PicoQuant) for time-resolved measurement. Images were acquired and analyzed using the SymPho Time software (Picoquant). The photons that were collected in the autofluorescence image were used to construct a global histogram to analyze fluorescent decay. The fluorescence decay was modeled using a double-exponential decay function and convoluted with the instrument response function (IRF), which was determined experimentally from the SH signal and had an FWHM of around 330 ps. The average lifetime was calculated as an intensity-weighted sum of the two lifetime components, according to Eq. (1),

$$\tau_{av} = \frac{a_1 \times \tau_1^2 + a_2 \times \tau_2^2}{a_1 \times \tau_2 + a_2 \times \tau_2}, \quad (1)$$

where τ_1 and τ_2 are the fluorescence decaying constants, calculated by data analysis, and a_1 and a_2 are the corresponding pre-exponential factors [23]. The presented FLIM images were binned to 128 × 128 pixels (from 512 × 512 pixels) to facilitate lifetime analysis. The color and brightness represent average lifetime and intensity, respectively.

3. Results and discussion

3.1. AF image and site-specific spectra of dental tissue

Figures 1 (A) and (B) show the 2-p autofluorescence images and the corresponding micro-spectra of the enamel and dentin, respectively, that were excited at 750 nm. AF spectra were obtained from selected regions in dentin and enamel. The SH signals are scaled down for display with the AF spectra. As in previous studies, in normal dental tissue, SH signals are obtained only from dentin but are almost invisible from enamel [2,9]. However, in a recent report, SH signals were also obtained from enamel owing to the strains around the cracks [3]. Both dentin and enamel emit broad and similar autofluorescence spectra from 400 to 600 nm, as presented in Fig. 1(B). The site-specific micro spectra (regions 4 and 5) from dentin for two-photon excitation at 750 nm exhibit the strong SH peak at 375 nm and the AF maximum around 470 nm. These spectra, obtained from different dentinal regions, do not significantly, differ, except in intensity. Under the same conditions, the emission spectrum of enamel has the AF maximum around 480 nm. Site-specific spectral profiles from enamel also do not vary significantly. Unlike AF in soft tissue, the AF in dental tissue is attributable to organic and inorganic components [4,29]. In Fig. 1 (A), the AF image of dentin reveals a tubular structure and is accompanied by SH signals that are associated with collagen molecules [2,9]. The

#137507 - $15.00 USD Received 2 Nov 2010; revised 7 Dec 2010; accepted 16 Dec 2010; published 17 Dec 2010

composition of enamel, however, differs from that of dentin. Enamel contains a high percentage of mineral materials but the organic components are present only in the interprismatic regions. However, the origin of AF in enamel remains unclear [24]. The inorganic components could be responsible for AF with peaks at 460 nm and 560 nm under single-photon excitation at 375 nm [29]. The two-photon excited AF spectra of enamel obtained herein include no peak around 560 nm, and reveal different spectral characteristics from the corresponding single-photon excited AF spectra [29,30]. The difference between the single- and two-photon fluorescence of enamel may be explained by the different excitation mechanism involved. Enamel exhibits AF close to the dentioenamel junction (DEJ), shown in Fig. 1(A). However, the site-specificity of the organic matrix component suggests that the organic matrix is important, as revealed by the intensity contrast among regions 1, 2 and 3. The characteristic enamel rods structure is clearly observed in the high-resolution autofluorescence image in Fig. 2 (A). These auto-fluorescing rods extend around 200 μm from the DEJ toward the enamel surface. The enamel rods are formed by ameloblast cells that elongate along the dentinoenamel junction, which process is known as Tomes' process [1]. The difference between the enamel features in Figs. 1(A) and Fig. 2(A) are attributed to the different orientation of the dental sections.

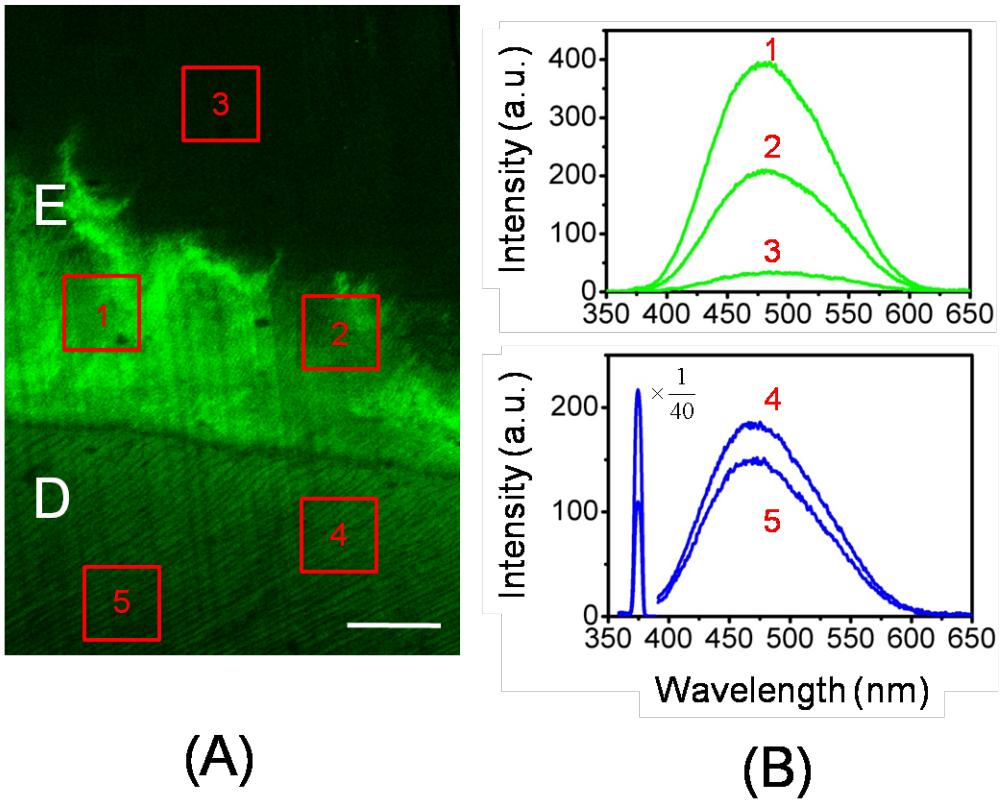

Fig. 1. (A) The autofluorescence image near dentin-enamel junction. Dentin tubules and enamel prisms can be seen clearly. Both dentin and enamel emit strong autofluorescence under two-photon excitation. E: enamel, D: dentin. (B) The AF spectra are obtained from 5 selected regions in enamel (green) and dentin (blue). The SH at 375 nm appears only in dentin. The scale bar is 100 μm

#137507 - $15.00 USD Received 2 Nov 2010; revised 7 Dec 2010; accepted 16 Dec 2010; published 17 Dec 2010

3.2. FLIM of sound and carious dental tissue

Figure 2 present the results of the FLIM investigation of the dental section. In addition to the evident intensity contrast, fluorescence lifetime analysis can be performed an image contrast by color-coding the fluorescence decaying constant (τ), reflecting changes in the energy relaxation pathways and nano-environments [17,18]. As shown in Fig. 1, dentin and enamel cannot be effectively differentiated by autofluorescence intensity mapping alone, owing to their similar spectral profiles. However, dentin and enamel exhibit distinct AF lifetime distributions, as presented in Fig. 2(B). The average AF lifetime in enamel falls in the shorter lifetime region of the lifetime histogram in Fig. 2(C). In comparison, the autofluorescence of dentin has a longer lifetime than that of enamel. Figure 2(D) also compares typical AF decay curves of dentin and enamel. These decay curves were well-fitted using the double-exponential model, as shown in Fig. 2(E). These results suggest that the difference between the lifetimes of AF from dentin and enamel arises from their different compositions [4]. Enamel is composed of around 96% inorganic material, mainly hydroxyapatite crystallites with traces of organic matrix, which envelopes each crystallite. In contrast, dentin consists of about 70% inorganic material and 30% organic material and water, major organic constituent is collagen [1,4]. The origins of autofluorescence from dental tissue may be quite diverse, and include both organic and inorganic components [4,29].

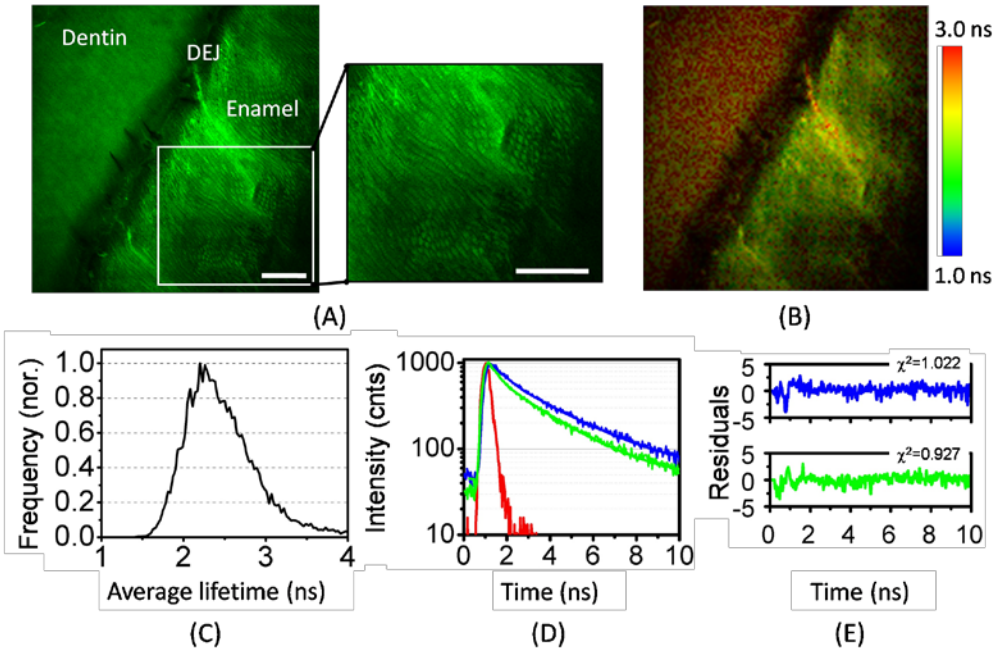

Fig. 2. (A) High resolution autofluorescence image near dentinoenamel junction and enlarge view of the selected region in enamel. DEJ: dentinoenamel junction. The scale bar is 50 μm. (B) the corresponding FLIM image; 128 × 128 pixels. The average autofluorescence lifetime is indicated in rainbow scale. (C) The average autofluorescence lifetime histogram obtained from FLIM image. (D) Representative autofluorescence decay curves from dentin (blue), enamel (green). The IRF is shown in red. Theses decay curves are fitted with double-exponential model. Their corresponding residuals (indicating a good fit) after optimal fitting are also shown.

To assess potential clinical applications of the pesented method), 2-p FLIM is applied to the carious dental sample, as shown in Fig. 3 (A). The autofluorescence lifetime image in Fig. 3 (B)

#137507 - $15.00 USD Received 2 Nov 2010; revised 7 Dec 2010; accepted 16 Dec 2010; published 17 Dec 2010

shows a few cracks and cavities in both dentin and enamel. Caries weakens the structure of dental tissues by demineralization and degradation of the organic matrix. Although caries alters the autofluorescence spectrum [11–14], laser fluctuation and concentration of fluorophores can influence the intensity-based method of identifying caries. The FLIM image in Fig. 3 (B) indicates that the average autofluorescence lifetime decreases gradually from the sound to the carious area, both in dentin and enamel. Figures 3 (C) and (D) present line profiles that were obtained from Fig. 3 (B). In dentin, from point C1, through C2, to S, the reduced average lifetime gradually recovered from 1.5 ns to 2.5 ns (around point S). However, enhanced AF accompanied the reduction in fluorescence lifetime. Caries in dental tissues involved the destruction of tooth tissue and the accumulation of fluorophores, which alter the characteristics of the AF spectrum [14]. Besides molecules from food/drinks, the increase in AF in carious regions can be attributed to the accumulation of bacterial metabolism products [31–33]. A similar observation was made of enamel in Fig. 3 (D), although to a lesser extent, because enamel has greater mineralization and less porosity than dentin. The shortened lifetime has also been reported elsewhere [22–24], and attributed to variations in the chemical and physical conditions of the fluorophores [34].

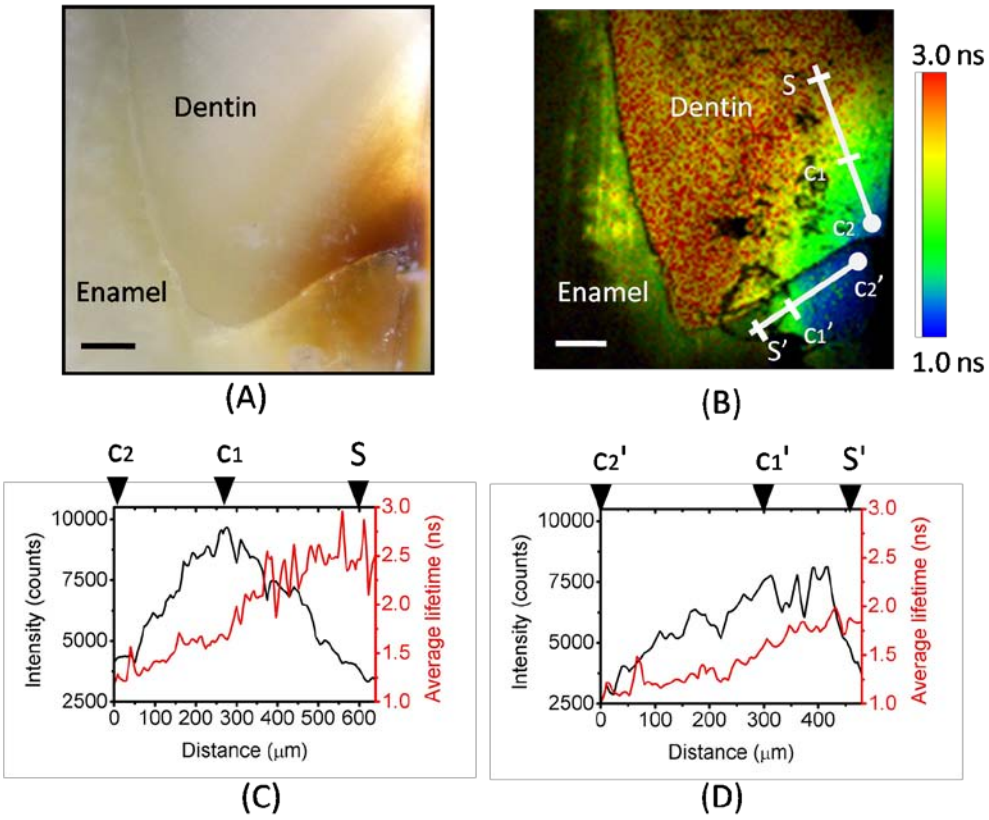

Fig. 3. (A) An epi-illuminated image of the carious dental sample used in this study. (B) the corresponding color coded FLIM image (binned to 128 × 128 pixels) that shows carious regions with greatly reduced lifetime (blue). The scale bar is 200 μm. The intensity (black) and average lifetime (red) line profiles obtain from FLIM image in (C) dentin and (D) enamel, respectively.

#137507 - $15.00 USD Received 2 Nov 2010; revised 7 Dec 2010; accepted 16 Dec 2010; published 17 Dec 2010

Figure 4 plots the autofluorescence decay curves obtained from points S-C1-C2 and S'-C1'-C2' in Fig. 3 (B). These curves were fitted by a double-exponential model and yielded the parameters $\tau_1 = 0.6$ ns, $A_1 = 38\%$, $\tau_2 = 2.8$ ns and $A_2 = 62\%$ at point S (sound dentin); $\tau_1 = 0.4$ ns, $A_1 = 63\%$, $\tau_2 = 2.3$ ns and $A_2 = 37\%$ at point C1, and $\tau_1 = 0.4$ ns, $A_1 = 71\%$, $\tau_2 = 1.9$ ns and $A_2 = 29\%$ at point C2 (carious dentin). In enamel, the obtained parameters were $\tau_1 = 0.4$ ns, $A_1 = 54\%$, $\tau_2 = 2.4$ ns and $A_2 = 46\%$ at point S' (sound enamel), $\tau_1 = 0.4$ ns, $A_1 = 62\%$, $\tau_2 = 2.2$ ns and $A_2 = 38\%$ at point C1', and $\tau_1 = 0.4$ ns, $A_1 = 75\%$, $\tau_2 = 1.8$ ns and $A_2 = 25\%$ at point C2' (carious enamel). The percentage of the short-lifetime component increased dramatically from the sound to the carious region in both dentin and enamel. These results suggest that caries- induced reduction in autofluorescence lifetime can be exploited to distinguish between healthy and carious teeth samples.

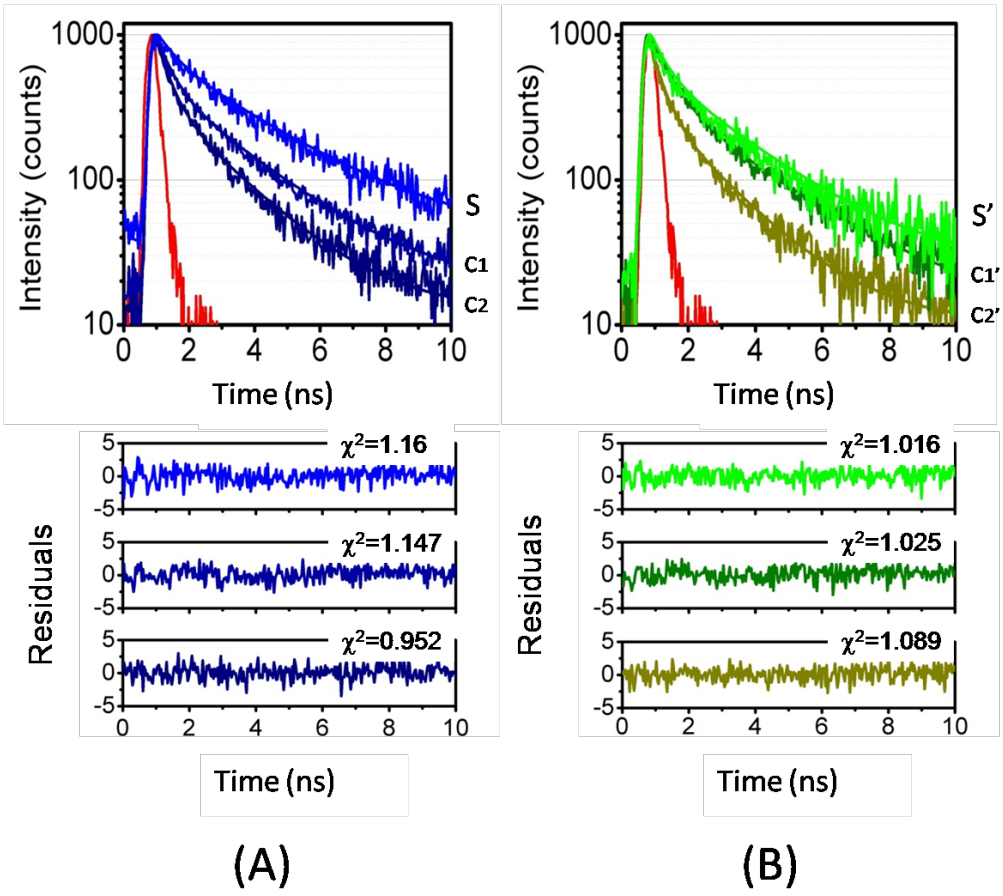

Fig. 4. (A) The autofluorescence decay curves from point S-c1-c2 and (B) S'-c1'-c2' shown in Fig. 3 (B). The IRF, taken with SH, is shown in red. These decay curves were fitted with double-exponential model. Their corresponding residuals (indicating a good fit) after optimal fitting are also shown.

3.3. Mineral density evaluation via micro-CT measurement

The formation of caries typically involves demineralization and the degeneration of the organic matrix. To evaluate the mineral loss that is caused by caries, micro-computed tomography (micro-CT) was utilized herein to quantify the mineral density of the carious dental samples that

#137507 - $15.00 USD Received 2 Nov 2010; revised 7 Dec 2010; accepted 16 Dec 2010; published 17 Dec 2010

were studied in the FLIM experiment. Micro-CT has been demonstrated to be able to characterize and quantify the mineral densities of sound and carious dental tissue [35]. The contrast in micro-CT images reflects the spatial distribution of linear attenuation coefficients, determined by the absorption of X-rays and the atomic composition of the sample. Hence, the mineral concentration or distribution in dental hard tissue can be evaluated both qualitatively and quantitatively via micro-CT measurement [36]. Enamel contains more mineral materials than does dentin, which difference is reflected by the major image contrast in Fig. 5 (A). The X-ray micro-CT image was taken in the same field of view as the FLIM image in an attempt to link the AF lifetime reduction to demineralization in carious regions. The line profiles that are indicated by arrows in Fig. 5 (A) were obtained and used to calculate the relative mineral density in Fig. 5 (B). Based on the assumption that the X-rays are absorbed by hydroxyapatite [37], the gray value was compared to that obtained from a pure hydroxyapatite disk that was scanned with the same parameters. The gray values were converted to relative mineral density. The relative mineral densities in the carious regions of both dentin and enamel are lower than those in the less carious/demineralized regions, and then return gradually to the values in the normal regions. This trend is consistent with the AF lifetime reduction in Figs. 3 (C) and (D).

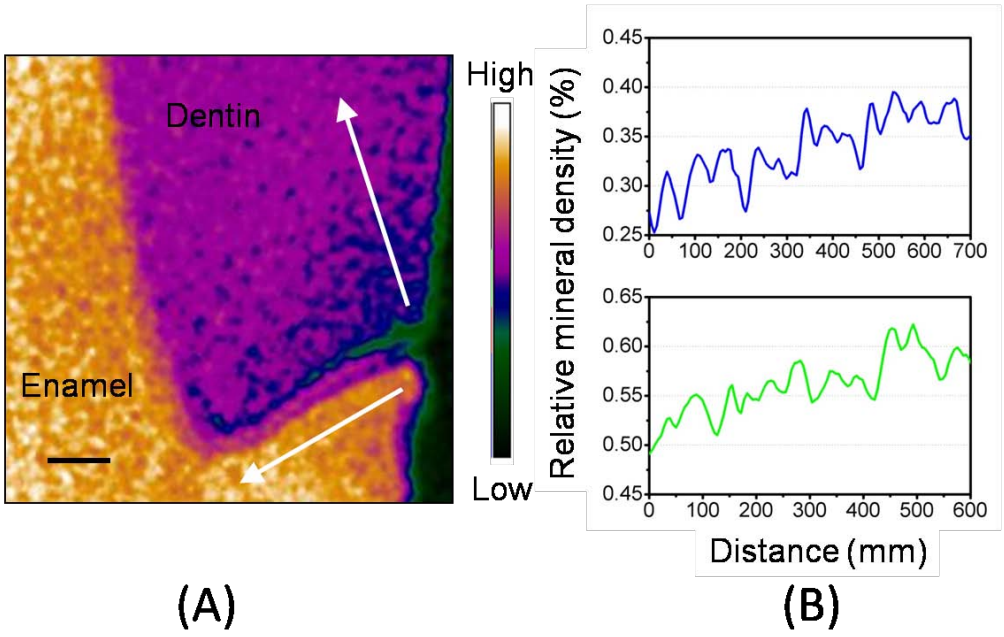

Fig. 5. (A) X-ray micro-CT image of the same carious dental sample shown in Fig. 3. The scale bar is 200 μm. (B) The relative mineral density in dentin (blue line) and enamel (green line) were calculated from the line profile indicated in micro-CT image.

4. Conclusion

The multiple modalities of multiphoton microscopy provide a powerful means of visualizing dental tissues, in both healthy and carious samples. The progressive demineralization of dental tissues is clearly reflected in their AF lifetime, which relationship was supported by micro-CT evaluation. These findings may provide an important basis for potentially valuable applications in the clinical diagnosis of dental caries.

#137507 - $15.00 USD Received 2 Nov 2010; revised 7 Dec 2010; accepted 16 Dec 2010; published 17 Dec 2010

Acknowledgements

This work is generously supported by the National Science Council, Taiwan under grants NSC 97-2112-M-010-002-MY3 and NSC 98-2112-M-010-001-MY3 and research grant R-222-000-015-305 from the Biomedical Research Council, Singapore. Additionally, Ted Knoy is appreciated for his editorial assistance.

#137507 - $15.00 USD Received 2 Nov 2010; revised 7 Dec 2010; accepted 16 Dec 2010; published 17 Dec 2010